ACS Sustainable Chemistry & Engineering

Research Article

pubs.acs.org/journal/ascecg

Fabrication of a Mixed Matrix Membrane with in Situ Synthesized Quaternized Polyethylenimine Nanoparticles for Dye Purification and Reuse

Junyong Zhu,[†] Yatao Zhang,*[,†,‡] Miaomiao Tian,[†] and Jindun Liu*[,†]

[†]School of Chemical Engineering and Energy, Zhengzhou University, Zhengzhou 450001, People's Republic of China

[‡]UNESCO Centre for Membrane Science and Technology, University of New South Wales, Sydney, New South Wales 2052, Australia

ABSTRACT: A facile and novel method for the fabrication of mixed matrix membranes (MMMs) has been developed, i.e., in situ synthesis of quaternized polyethylenimine (QPEI) soft nanoparticles (SNPs) followed by quaternization with bromoethane in poly(ether sulfone) (PES) casting solution. The resulting composite membranes were constructed via phase inversion method. The influences of SNPs on the morphology and performance of the hybrid membranes were systematically investigated by scanning electron microscopy, dynamic water contact angle, antifouling measurement, etc. The composite membranes exhibited a thin top layer and porous finger-like structure, which were greatly affected by in situ synthesized SNPs. Contact angle and water uptake measurements indicated that the hydrophilicity of hybrid membranes markedly improved in contrast with that of unfilled membrane. Meanwhile, the water flux of the membranes significantly enhanced due to the incorporation of SNPs. The ion-exchange capacity (IEC) value could achieve as high as 0.72 mmol g^{-1} with an initial PEI content of 1.5 wt %. The salts rejection of MMMs followed the order: $MgCl_2$ > $MgSO_4$ > Na_2SO_4 > NaCl, confirming that the hybrid membranes were positively charged. Meanwhile, the fouling parameters demonstrated that the composite membranes exhibited a preferable antifouling property. The newly developed membranes demonstrated an impressive prospect for the dye purification due to the high rejection of reactive dyes with a high permeation flux, as well as low multivalent ions retention. The possible separation mechanism of dyes and salts for composite membranes influenced by synthesized SNPs was also proposed in this study.

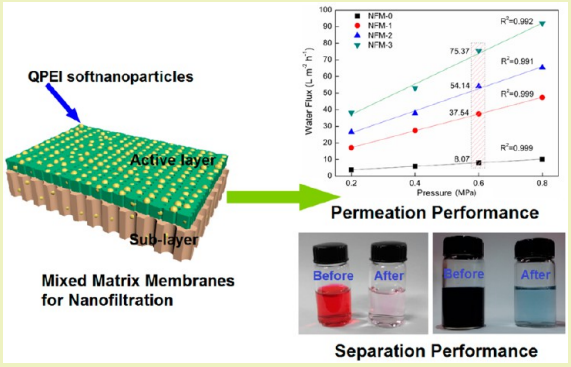

KEYWORDS: *Polyethylenimine, in situ synthesis, mixed matrix membranes, soft nanoparticles, antifouling property, dyes purification*

INTRODUCTION

The increasing volumes of discharges of dye effluents to aquatic environments have gained growing concern because most of them are nonbiodegradable, generally quite toxic, and even consume the dissolved oxygen that is essential to aquatic life.[1−4] It is estimated that the dye loss is about 10−15% in the dyeing process, specifically, 200−350 m^3 of dye wastewater is generated to produce 1.0 ton of available product in the textile industry.[5] Thus, inadequate removal of the dyes wastewater before their release into the environment, especially to water systems, would not only contaminate fresh water resources, thus posing a risk to human beings, but also restrain light permeation, having an adverse influence on aquatic life.[6−8] Therefore, numerous ongoing research efforts attempt to achieve an effective removal of dyes from wastewater.[9−12] Meanwhile, in the dyeing procedure, inorganic salts including sodium chloride (NaCl, ∼6.0 wt %) and sodium sulfate (Na_2SO_4, ∼5.6 wt %) have been extensively used to enhance the dye uptake of the fabric. A mass of wastewater containing salts and dyes need to be treated and separated with effective methods for dye desalination and reuse.[13] Additionally, in the dye synthesis process, some inorganic salts (NaCl) existed in synthetic dyes must be removed to improve dyes quality and stability.[14] The conventional route (salting-out) applied in dye purification is bound to produce a great deal of wastewater with high salinity in this process.[15] Therefore, the separation of dye and inorganic salt has aroused broad concern in view of dye desalination, reuse and purification both in the synthetic and dyeing processes.[16,17]

As an alternative candidate for wastewater treatment technology, membrane separation is deemed to be environmentally friendly, easy to control and operate, as well as low initial investment and consumption energy.[18−21] Hereinto, nanofiltration (NF) represents one of the most active separation and purification fields extensively employed in the applications of water softening, dye desalination, pharmaceut-

Received: January 5, 2015
Revised: March 4, 2015
Published: March 10, 2015

DOI: 10.1021/acssuschemeng.5b00006
ACS Sustainable Chem. Eng. 2015, 3, 690−701

icals, wastewater reclamation, etc.[22−27] Nanofiltration is a liquid-phase pressure-driven separation process, with pore size in the nanometer range (0.5−2 nm) and molecular weight cutoff (MWCO, molecular weight of solute that is 90% rejected by the membrane) varying from 100 to 1000 Da.[28−31] Its major separation mechanism involves steric hindrance exclusion, electrostatic interaction (Donnan effect) and solute-membrane affinity. When applied in the treatment of dye wastewater, traditional dense nanofiltration membranes (NFMs) could reject both organic dyes and multivalent salts (SO_4^{2-}) that could not only decrease the quality of synthetic dye but also pose a big loss of valuable salts that could have been recycled.[32,33] Currently, positively or negatively charged and hydrophilic NFMs (stands for a radical alternative to conventional NF membrane) and have attracted considerable attention primarily ascribed to the improvement of antifouling property and better permeation flux.[34]

Poly(ether sulfone) (PES) is a commercially available, structurally stable polymer widely applied in high-performance applications principally to the excellent combination of superior pH and chlorine tolerance, high mechanical strength, and good thermal resistance.[35−38] One issue with virgin PES membrane is relative high hydrophobicity ascribed to its repeated ether and sulfone linkage alternating between aromatic rings. It is found that hydrophobic membrane surface is vulnerable to the foulant adhesion and contamination, thus notably limiting its further application in control of water system. The priority is to optimize the morphology and performance (hydrophilicity, roughness, charge property, etc.) of membrane without affecting their processability. There are various approaches to fabricate NFMs, such as blending,[39,40] coating,[41,42] graft polymerization[43,44] and interfacial polymerization (IP).[45,46] However, processes such as surface grafting are difficult to control and their production costs are relative high, and these methods often involve multiple steps, which are also unfriendly to the environment. Blending existing polymers with hard inorganic compounds usually generates a defect polymer/inorganic particle interface due to the decreased compatibility, and even produces undesired agglomeration, thus notably decreasing membrane separation performance.[47] Hence, an advanced composite membrane should fulfill the following requirements: selecting an ideal filler to match the polymer matrix or constructing the desired polymer−filler interface.[48] Soft nanoparticle (SNP) or polymeric nanoparticle used as promising nanofiller has a better compatibility with polymer matrix than hard inorganic fillers.[49] Furthermore, the method of in situ synthesis could endow polymer with better filler/polymer interface than simple blending modification due to dissolved precursor cross-linking and growing to form SNPs in casting solution.

Recently, a facile route to the preparation of mixed matrix polyvinylidene fluoride (PVDF) membranes embedded with PEI particles obtained from in situ synthesis using ECH as cross-linker.[50] In this study, we reported a novel method with respect to in situ synthesis of QPEI SNPs in PES casting solution using epichlorohydrin as cross-linker and bromoethane as modifying agent. The composite membranes were prepared via phase inversion method. The advantages of fabrication approach are as follows: ease of controlling and processing, simplicity, compact organic filler−polymer interaction, and homogeneous distribution of nanoparticles. The type of composite membrane using the method could realize the perfect fractionation of low molecular weight (LMW) dyes and salts (NaCl, Na_2SO_4, etc.) with a high flux. Therefore, the prepared membranes should be amenable to the potential application in dye purification and reuse. The effects of SNPs on the membrane surface hydrophilicity, microstructure, permeation and antifouling property were investigated in detail. Additionally, a possible separation mechanism of as-prepared membranes was proposed in this work.

EXPERIMENTAL SECTION

Materials. Poly(ether sulfone) (PES, Mw = 55 000 Da) was obtained from BASF Company, Germany. *N*-dimethylacetamide (DMAc) and supplied by Tianjin Kewei Chemical Reagent Co. Ltd., China. Branched polyethylenimine (PEI, Mw = 25 000 Da), epichlorohydrin, bromoethane and bovine serum albumin (BSA) was purchased from Sigma-Aldrich. Reactive red 49 (Mw = 576.49 Da) and reactive black 5 (Mw = 991.82 Da) were obtained from Sunwell Chemicals Co., Ltd., China and the structural formulas (Figure 1) were reported by our previous work.[34] All other solvents and reagents of analytical grade were purchased from Tianjin Kermel Chemical Reagent Co., Ltd., China and used without further purification. Deionized water was used throughout all experiments.

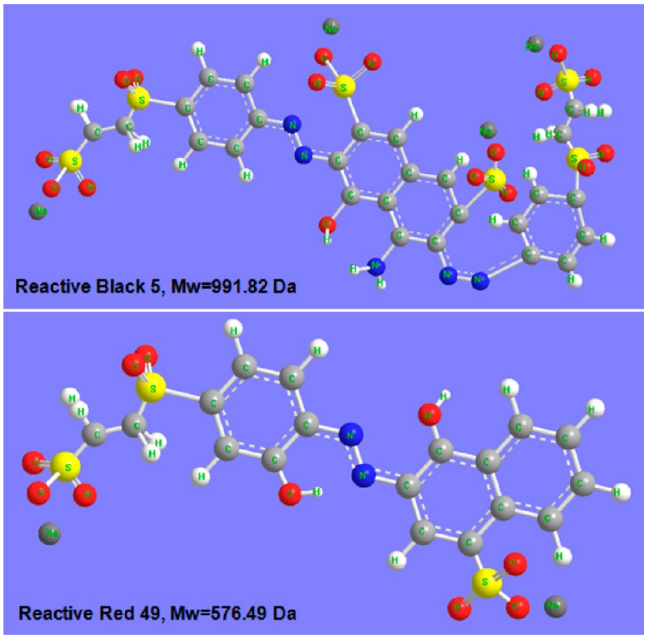

Figure 1. Molecular structures of Reactive Red 49 and Reactive Black 5.

Preparation of Composite Membranes. The procedures and reaction schemes for the preparation of mixed matrix membranes with in situ generated and quaternized PEI nanoparticles are shown in Figure 2. First, a certain amount of PEI was well dissolved into DMAc with ultrasonic treatment for 30 min. The above solution was mixed with PES under continuous stirring at 50 °C for 5 h, forming a uniform casting solution. Second, the required quantity of epichlorohydrin dissolved in DMAc was added into the solution followed by cross-linking reaction at 70 °C for 6 h under nitrogen atmosphere. Subsequently, a certain amount of bromoethane dissolved in DMAc was added into above mixture and stirred at 65 °C for 2 h of quaternization. Finally, the resulting yellow suspension was stirred for another 10 h at room temperature to achieve optimal dispersion of PEI particles in PES matrix solution. The casting solution was degassed under vacuum at 40 °C. And the compositions of the casting solution are shown in Table 1.

After degasification, the achieved homogeneous solution was poured on a clean glass substrate. A casting knife (with 100 nm air

DOI: 10.1021/acssuschemeng.5b00006
ACS Sustainable Chem. Eng. 2015, 3, 690−701

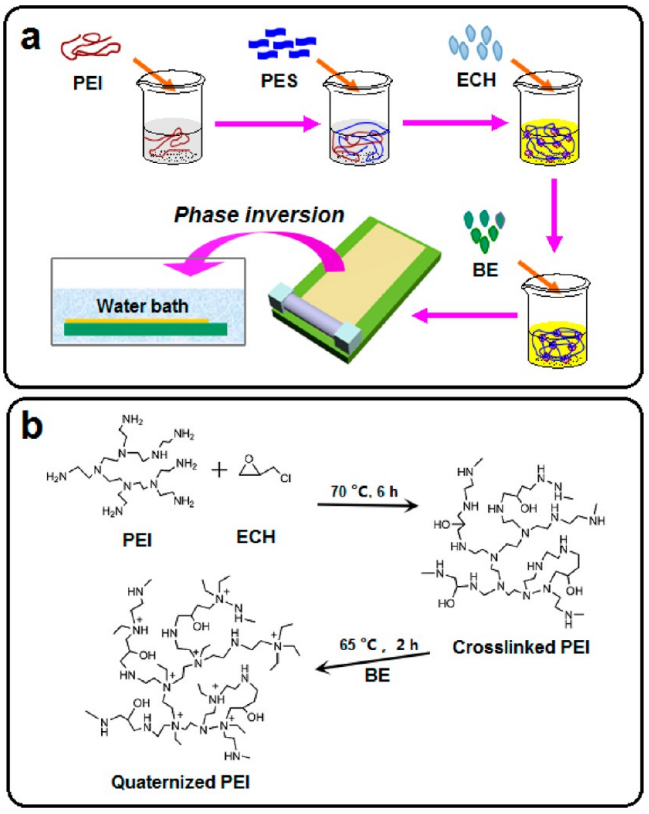

Figure 2. Procedures and reaction schemes for the preparation of mixed matrix membranes with in situ generated and quaternized PEI nanoparticles. (a) Procedure of mixed matrix membrane via phase inversion method; (b) reaction schemes of in situ generated and quaternized PEI nanoparticles.

Table 1. Compositions of the Casting Solutions

membrane	NFM-0	NFM-1	NFM-2	NFM-3
PES (wt %)	21	21	21	21
PEI (wt %)		0.5	1.0	1.5
epichlorohydrin (wt %)		1.0	1.0	1.0
bromoethane (wt %)		0.05	0.05	0.05
DMAc (wt %)	79	77.45	76.95	76.45

gap) was used to uniformly cast the solution consist of PEI particles onto substrate, which was subsequently immersed into coagulation bath (deionized water, 25 °C) for precipitation. Finally the resulting membranes were kept in deionized water, which was replaced every day. The membranes prepared with different PEI content of 0, 0.5, 1 and 1.5 wt % for the total solution hereinafter are referred to as NFM-0, NFM-1, NFM-2 and NFM-3, respectively.

Characterization of the Prepared Membranes. Scanning electron microscopy (SEM) directly provides the visual information on the cross-sectional and plane morphology of the as-prepared membranes. SEM (JEOL Model JSM-6700F scanning electron microscope, Tokyo, Japan) was used in this work. The wet membranes were cut into small pieces and washed by fresh water, then blotted up with filter paper. The pieces were immersed in liquid nitrogen for a certain time and were frozen. Frozen fragments of the membranes were fractured and kept in air for drying. Finally, dried samples were gold sputtered and inspected with the microscope at 10 kV.

The ion exchange capacity (IEC, mmol g^{-1}) of the membranes was determined as follows. The dried samples (1 g) were cut into small pieces, which were immersed into NaCl solution (0.5 mol/L) for 48 h under shaking. Then the samples were washed by water for 3−4 times until there were no chloride and bromide ions, which could be tested using $AgNO_3$ solution titration. Subsequently, the obtained membranes were soaked into $NaNO_3$ solution (0.5 mol/L) and titrated with $AgNO_3$ solution with a known concentration.

The charge property of NFMs surface could be characterized by ζ-potential, which was measured via a streaming current method on an electrokinetic analyzer (Surpass Anton Paar, Austria). The area of each sample was 0.2 × 0.1 cm, and the selected flat membranes were immobilized to the adjustable gap cell. KCl solution (1.0 mmol/L) was used for the determination of the ζ-potential of the membranes, and several solutions were prepared to study membrane surface charge density influenced by various pH values of the solution. Hydrochloric acid (HCl) and potassium hydroxide (KOH) were used to adjust the pH value. The measurement progress was controlled by software named Visolab for Surpass, and the ζ-potential values were obtained by the software.

The hydrophilicity of membrane is quantified by measuring the contact angle formed between the membrane surface and water. The dynamic contact angles were measured as the contact time varying. The water contact angle of the membrane was obtained by using a contact angle goniometer (OCA20, Dataphysics Instruments, and Germany) at room temperature and 50% relative humidity. All contact angle measurements were made using 5 μL of deionized water. To make the contact angle more persuasive, the contact angle was measured at five random locations for each sample and the average was determined.

The as-prepared samples (ca. 1 g) were dried under vacuum at 30 °C until constant weight and then immersed in water for 24 h. After that, the weight of wet membranes (W_w), whose surface was mopped using the blotting paper, was noted down. Finally, the membranes were completely dried anew under vacuum at 30 °C. The water uptake (W_r) can be calculated by the following equation:

$$W_r = \frac{W_w - W_d}{W_d} \times 100\% \quad (1)$$

where W_w is the weight of wet membrane after dried by blotting paper and W_d is the weight of the dried membrane.

Separation Performance of Membranes. Quaternized PEI particles embedded nanofiltration membranes were characterized by measuring the pure water flux, salt rejection and dyes retention. The permeation performance of the NFMs was investigated with a cross-flow module at room temperature in the range of 0.2−0.8 MPa with an effective membrane area of 28.26 cm^2. Each tested membrane was initially pressurized with pure water at 0.6 MPa for 30 min to reach a steady state before testing. The detailed operation of the NF setup is similar to our earlier works.[51−53] After compacted, the pure water flux values were recorded at ambient temperature at 0.2, 0.4, 0.6 and 0.8 MPa, respectively. The water flux J (L m^{-2} h^{-1}) was calculated by the following equation:

$$J = \frac{V}{A \times \Delta t} \quad (2)$$

where V (L) is the volume of permeated water, A (m^2) is the effective area of the membrane and Δt (h) is the permeation time. The feed solution (1 g/L) including NaCl, $MgCl_2$, Na_2SO_4 and $MgSO_4$ were forced to permeate through the membrane and the permeates were collected subsequently. Finally, the rejection experiments of water-soluble dyes (Reactive Red 49, Reactive Black 5, 0.5 g/L) were performed after the system was rinsed cleanly with deionized water. In addition, the concentration of saline solution was measured with an electrical conductivity meter (DDS-11A, Shanghai Hongyi Instrument Co. Ltd., China). The concentration of the water-soluble dyes was determined by a UV−vis spectrophotometer (Shimadzu, Japan). The rejection (R) and permeation (P) of salts and dyes were obtained by

$$R = \frac{C_f - C_p}{C_f} \quad (3)$$

$$P = 1 - R \quad (4)$$

where C_p and C_f represent both salt and dye concentrations in the permeate and feed, respectively. The mean pore size of the selective

DOI: 10.1021/acssuschemeng.5b00006
ACS Sustainable Chem. Eng. 2015, 3, 690−701

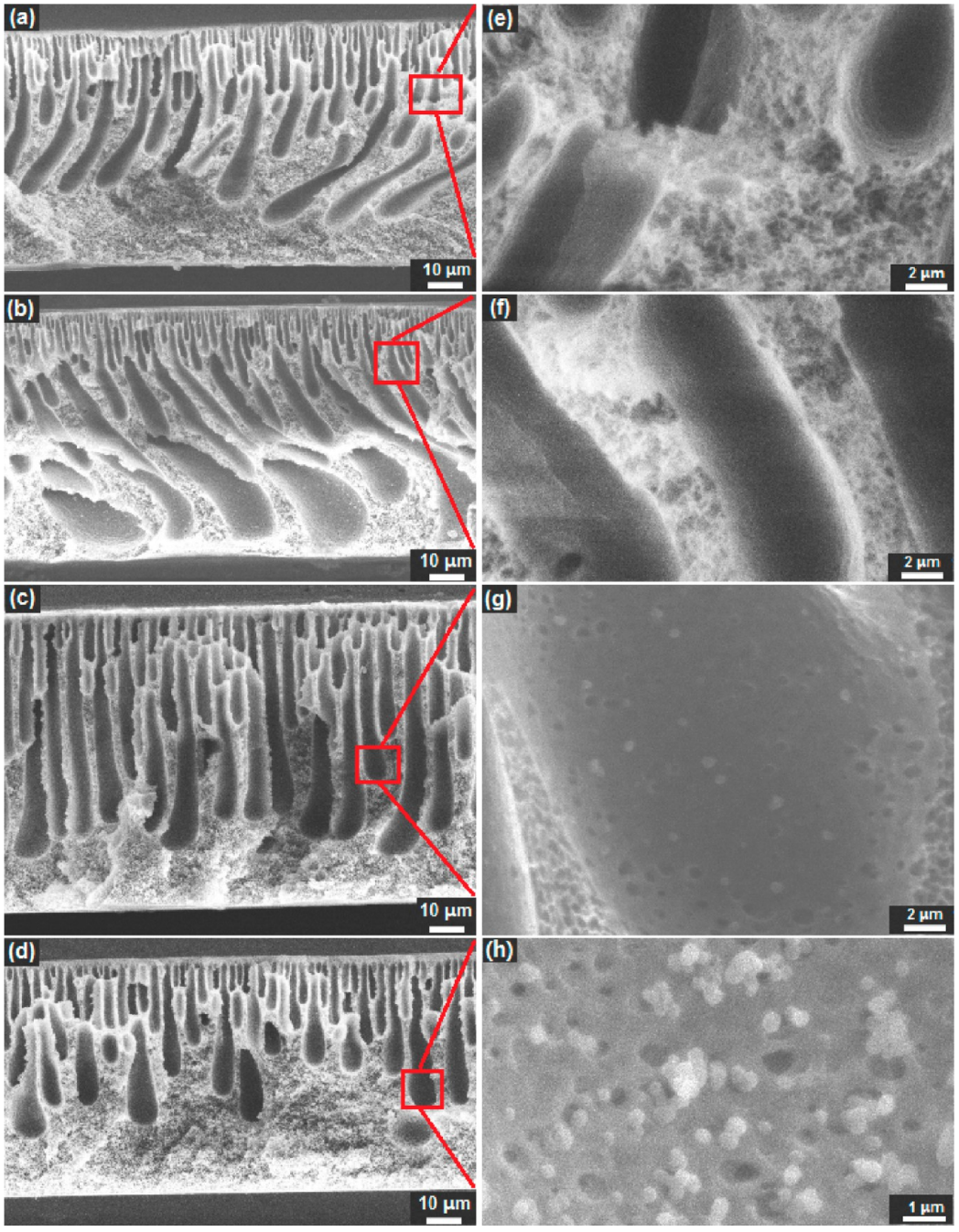

Figure 3. Cross-sectional SEM images of loose nanofiltration membranes prepared with the addition of the following concentrations of PEI nanoparticles: (a, e) 0, (b, f) 0.5, (c, g) 1 and (d, h) 1.5%.

layer, one of the vital factors to reflect the permeation properties (size effect), was correlated with the molecular weight cutoff (MWCO) of PEG[34] and the equation is shown as follows

$$y = -5E - 8x^2 + 5E - 4x + 0.3319 \quad (5)$$

where y represents Stoke's radius and x is the MWCO of PEG for membrane. Herein, the same concentration of PEG solution with different molecular weights (400, 600, 800, 1000, 1500 and 2000 Da) was selected to estimate the MWCO of prepared membranes. The filtration operation was under 0.4 MPa and the MWCO value was determined corresponding to the rejection of PEG solution being up to 90%.

Antifouling Performance Measurements. The antifouling performance of NF membranes was investigated with BSA (1 g/L) solution (PBS, 0.1 mol/L, pH 7.0) at room temperature and 0.4 MPa. In a typical procedure, pure water was first filtered through the membrane, rendering the system stable before use. Then pure water filtrated through the membrane for 60 min and the average water flux was recorded as $J_{w,1}$. After water flux tests, the stirred cell was rapidly refilled with protein solution and keeping for another 60 min and the flux for BSA solution was measured as J_p. After that, the membrane was washed thoroughly with deionized water for 30 min (the washing time was not counted in the filtration cycle). The water flux ($J_{w,2}$) of the cleaned membranes was measured until the system was stable. The antifouling performance evaluation for each membrane was operated with three cycles. To evaluate the antifouling property of membranes, the flux recovery ratio (FRR) and the total fouling ratio (R_t) were calculated by the following equation:

DOI: 10.1021/acssuschemeng.5b00006
ACS Sustainable Chem. Eng. 2015, 3, 690−701

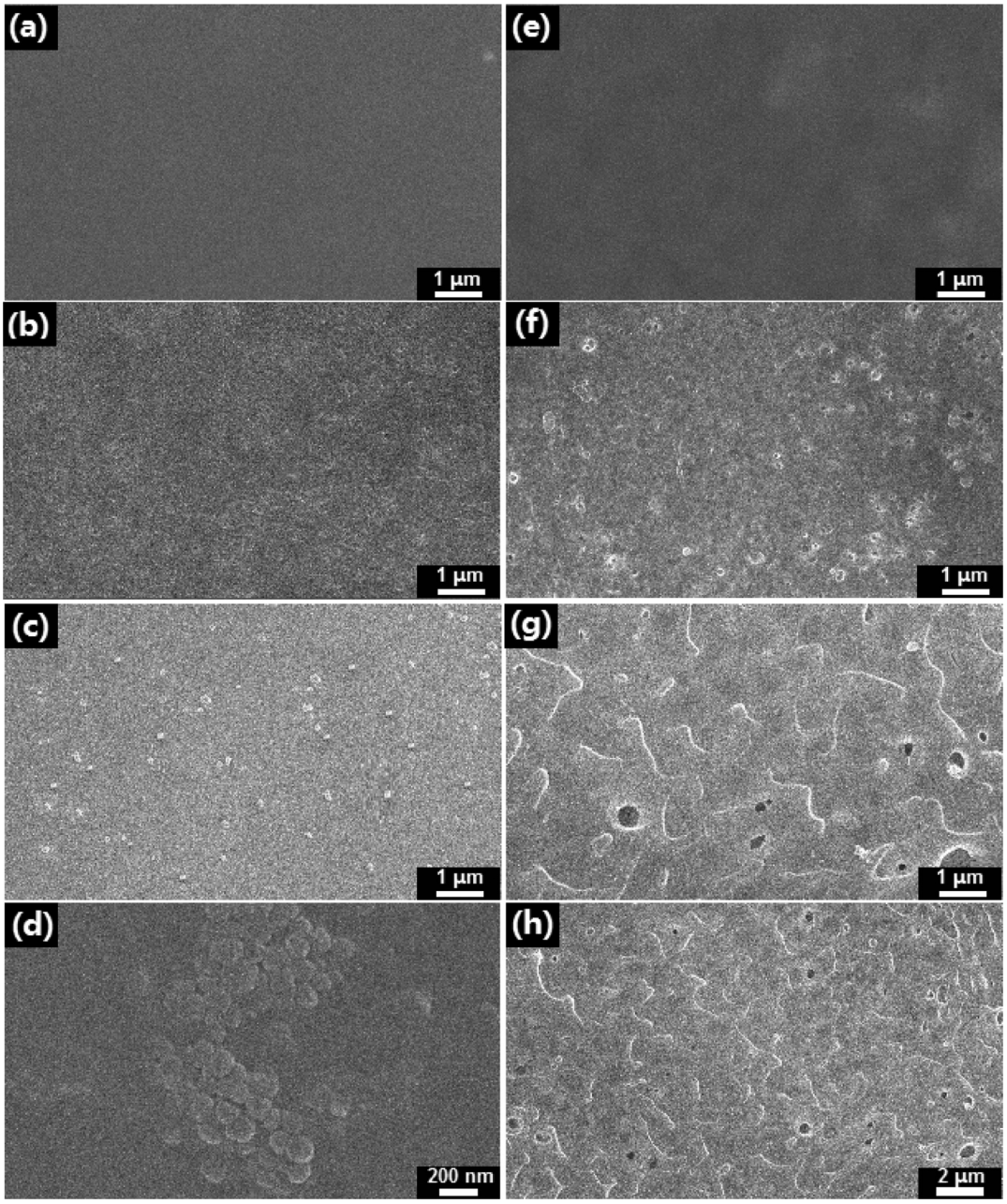

Figure 4. Top (a–d) and bottom (e–h) layers SEM images of loose nanofiltration membranes prepared with the addition of the following concentrations of PEI nanoparticles: (a, e) 0, (b, f) 0.5, (c, g) 1 and (d, h) 1.5%.

$$\mathrm{FRR} = \frac{J_{w,2}}{J_{w,1}} \times 100\% \tag{6}$$

To analyze the fouling process in detail, total fouling ratio (R_t) is the degree of total flux decline caused by total fouling. Reversible fouling describes the fouling caused by concentration polarization and irreversible fouling is ascribed by adsorption or deposition of protein molecules. Reversible fouling ratio (R_r) and irreversible fouling ratio (R_{ir}) were calculated using the following equations:

$$R_t(\%) = \left(1 - \frac{J_p}{J_{w,1}}\right) \times 100\% \tag{7}$$

$$R_r(\%) = \left(\frac{J_{w,2} - J_p}{J_{w,1}}\right) \times 100\% \tag{8}$$

$$R_{ir}(\%) = \left(\frac{J_{w,1} - J_{w,2}}{J_{w,1}}\right) \times 100\% = R_t - R_r \tag{9}$$

RESULTS AND DISCUSSION

Morphology of Membranes. The cross-sectional SEM images of loose nanofiltration membranes are shown in Figure 3. The images in Figure 3a–d exhibit a typical thin top-layer supported by the finger-like porous sublayer cavities. This result has been observed in related literatures.[39,40] It was widely accepted that high mutual diffusivity between water (non-solvent) and DMAc could promote forming an asymmetric structure during the phase inversion process.[54] The thicknesses of NFM-0, NFM-1, NFM-2 and NFM-3 were about 0.93, 1.10, 2.33 and 1.67 μm, respectively. The membranes fabricated by

DOI: 10.1021/acssuschemeng.5b00006
ACS Sustainable Chem. Eng. 2015, 3, 690–701

adding 0.5 wt % PEI (Figure 3b) exhibited the larger pore channels and better pore connectivity through the whole membranes compared with nascent PES membrane. It can be explained by the SNPs containing many types of hydrophilic groups, which could also accelerate the exchange rate of solvent and nonsolvent during phase inversion. Additionally, the existence of SNPs could substantially increase the thermodynamic instability of the casting solution, thus giving rise to a rapid mass transfer rate in the phase inversion process. However, when the adding amount of PEI increased over 1 wt % (Figure 3c,d), the thickness of the skin layer obviously increased and the size of finger-like macrovoid reduced compared with NFM-1. As we all know, two factors (hydrophilicity and viscosity) competitively functioned as forming the porous and loose embedded membranes.[39] The viscosity of the casting solution increased due to a further increase of as-formed SNPs, which impaired water (nonsolvent) inflow during phase inversion, hence, rendering a delayed exchange of solvent and nonsolvent as well as suppressing the formation of large pore size.[52,55] Figure 3g,h exhibited a cross-sectional images magnified from NFM-3 and NFM-4. It was found that SNPs with the diameter of ca. 200 nm existed in the finger-like microvoids and the holes around them were the similar size. The holes were formed induced by synthesized SNPs that acted as the pore-forming agent, thus could improve the water permeability in contrast of unfilled PES membrane.

The SEM images of the top and bottom layers of unfilled PES and composite membranes are shown in Figure 4. As seen from Figure 4a,e, the unfilled membrane exhibited a thin dense top layer and a smooth bottom layer without the obvious macrovoid. When the PEI content increased to 0.5 wt %, a relative loose structure of the top layer (Figure 4b) and certain amount of SNPs appeared on the bottom layer (Figure 4f). This result can be explained as follows. The larger SNPs migrated toward the bottom of membrane in the process of phase inversion and as above-mentioned the presence of hydrophilic SNPs increase the mass transfer rate between solvent and nonsolvent, thereby forming a porous and loose structure. When the added content of PEI reached 1 wt %, SNPs (ca. 200 nm) emerged on the top layer (Figure 4c) due to the migration of hydrophilic particles during phase inversion. The lines and wrinkles that resembled the leaf texture existed in the bottom layer (Figure 4g,h). This result may be due to the subsidence caused by SNPs because of an excess of PEI precursor. Similarly, Figure 4d manifests the partial aggregation of PEI particles when the concentration of PEI reached up to 1.5 wt %. In summary, the in situ generated SNPs endow the hybrid membrane with more porous and looser structure, which could benefit the water permeability. The smaller size of SNPs migrated toward the top layer during phase inversion, rendering modified membranes better hydrophilicity, corresponding to the results of contact angle and water uptake.

Hydrophilicity and Charged Characteristics of Membranes. Due to the hydrophilic SNPs in the polymeric membrane matrix, both the hydrophilicity and water uptake of hybrid membranes achieved were optimal in comparison with that of an unfilled PES membrane. Hydrophilic surfaces are inclined to combine with water molecules due to the existence of hydrophilic groups, and thus can form a tightly bounded water layer, which is preferred for fouling reduction for hydrophobic foulants.[56] Therefore, hydrophilic surfaces could endow composite membranes with an improved antifouling property. Figure 5 presents the dynamic water contact angle data for unfilled PES membrane and hybrid membranes with

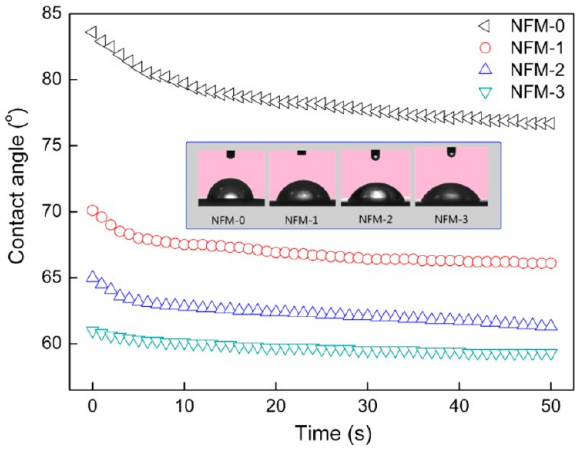

Figure 5. Dynamic water contact angles of NFM-0, NFM-1, NFM-2 and NFM-3.

different PEI contents. The initial contact angle of pristine PES membrane was 84.6°, which was similar to that of the PES membranes reported in related literature.[57,58] Compared with the unfilled PES membrane, the contact angle of the SNPs functionalized membranes decreased distinctly. When the PEI concentration increased to 1.5 wt %, the equilibrium value of the contact angle reduced to 58.9°, indicating a more hydrophilic material has been fabricated. It was generally accepted that the lower water contact angle showed a better hydrophilic property, that is, the composite membranes exhibited a superior hydrophilicity compared with that of unfilled membrane. The results of water uptake are shown in Figure 6. As seen from the figure, the values of water uptake for hybrid membranes considerably enhanced compared to unfilled PES membranes, which were consistent with the contact angle measurements. The water ratio of NFM-3 increased up to 233.6%, which was 130.8% higher than that of unfilled PES membrane. Conclusively speaking, in this case, the hybrid membranes exhibited a better hydrophilicity than unfilled membrane due to the embedded hydrophilic SNPs.

Charge capacity of NF membranes surface was evaluated by ion-exchange capacity (IEC), which is shown in Figure 6a. From Figure 6, the values of IEC were measured through exchanged Cl^- content and distinctly increased compared with unfilled membrane. The IEC values of NFM-1, NFM-2 and NFM-3 were 0.37, 0.61 and 0.72 mmol g^{-1}, respectively. The charge capacity of hybrid membranes enhanced with an increase of quaternized PEI concentration, thus apparently manifesting an excellent charged property for the hybrid membranes. Figure 6b exhibits different ζ-potentials of the pristine and hybrid membranes with various PEI concentrations. The NFM-0 and NFM-1 showed negative ζ-potentials in a wide range of pH values. Importantly, the isoelectric point of NFMs trended toward a higher pH value followed by increasing PEI concentration. That is, the hybrid NFMs presented an extensive positive charge property compared with negatively charged PES membranes. It was found that the charge density on surface of NFM-3 was higher than that of NFM-2. The enhanced charge density was mainly due to the increased growth of SNPs, which were positively charged. The results of ζ-potential measurements demonstrated that the

DOI: 10.1021/acssuschemeng.5b00006
ACS Sustainable Chem. Eng. 2015, 3, 690−701

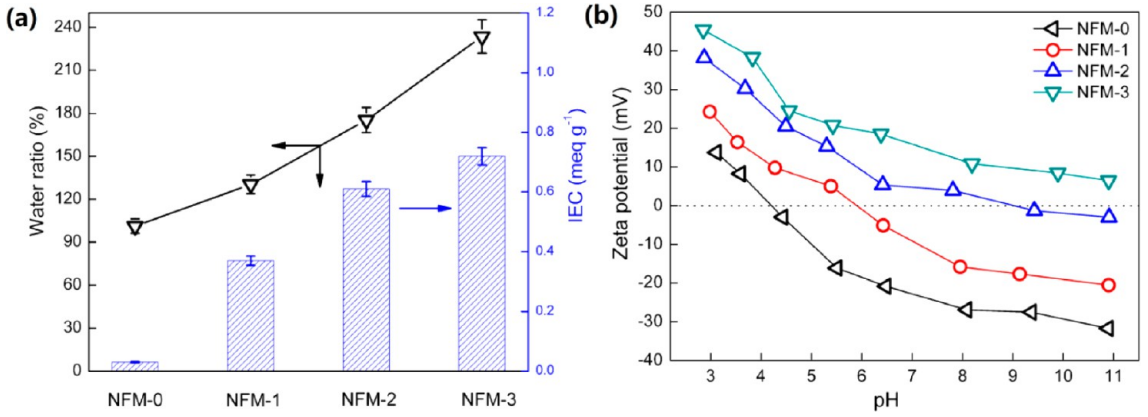

Figure 6. (a) Water ratio and ion-exchange capacity (IEC) of NFM-0, NFM-1, NFM-2 and NFM-3, (b) ζ-Potentials of NFM-0, NFM-1, NFM-2 and NFM-3 at different pH.

surface of composite NFMs was positively charged when PEI concentration was over 1.0 wt %.

Permeation Property of Membranes. The influence of SNPs on the permeability of unfilled and composite membranes under different pressure was examined, and the results are plotted in Figure 7. It was found that the pure water

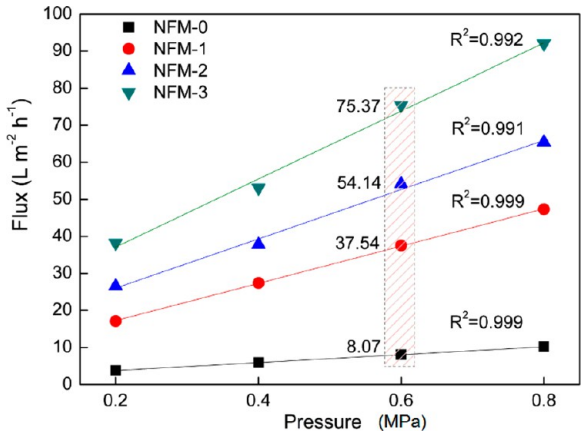

Figure 7. Effect of PEI nanoparticles content on the water flux of the hybrid membranes under various operation pressures.

flux of composite membranes greatly increased with an increase of adding amount of PEI concentration. In detail, the nascent PES membrane gave the lowest pure water flux of 8.07 L m^{-2} h^{-1}, whereas the NFM-3 reached up to 75.37 L m^{-2} h^{-1} at 0.6 MPa. The water permeation of membranes is generally influenced by surface hydrophilicity, internal structure and the pore size of the top-layer. In this work, the result can be explained by the improved hydrophilicity, loosely selective structure and porous macrovoid (Figures 4 and 5). Generally speaking, a hydrophilic surface could attract water molecules inside and the loose pore structure and porous macrovoid facilitated water permeation under certain pressure, giving rise to an enhanced water permeability compared with unfilled PES membrane. In addition, as-formed SNPs could undermine the polymer chain packing to a certain degree and increase the free volume between polymer chains, thus rendering interface voids around particles from the top layer, but in another sense improved the water permeability. In summary, the resulting hybrid membranes prepared by the in situ synthesis and phase inversion, exhibited fairly high water flux, which was caused by the loose structure and hydrophilic surface.

The rejections for PEG of the hybrid NF membranes with different HNTs-poly(NASS) contents (0-NF, 1-NF, 2-NF and 3-NF) are plotted in Figure 8. Moreover, the MWCO values of

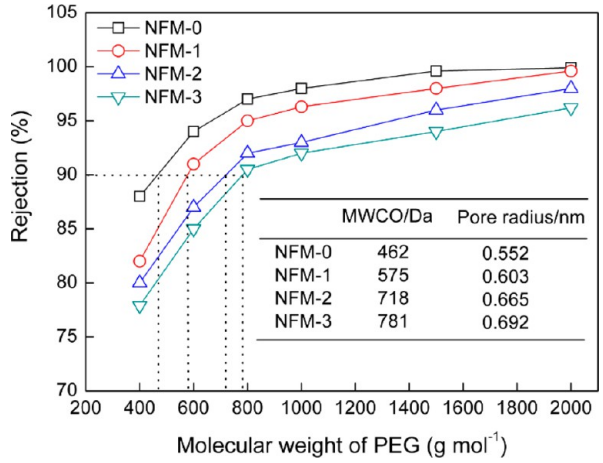

Figure 8. Effect of PEI concentration on MWCO of PEG and the Stoke's radius of membrane (inert).

membranes with different content were determined and the mean pore sizes of these membranes are shown in the table. As shown in Figure 8, it was concluded that the MWCO values of NFM-0, NFM-1, NFM-2 and NFM-3 were 462, 575, 718, and 781, respectively. The corresponding values of the mean pore radius (Stoke's radius) were calculated as follows: 0.552, 0.603, 0.665 and 0.692 nm, respectively. The results demonstrated that the mean pore size enhanced with an increase of PEI concentration. To explore the application of unfilled membrane and composite membranes for the treatment of textile dye wastewater, two types of dye solutions, Reactive Red 49 and Reactive Black 5, were used to investigate the separation performance of NF membranes. The selected dyes are negatively charged while they have different molecular weights. Figure 9 exhibits the rejection and permeation flux of dyes for NF membranes. It was apparent that all NF membranes presented an overall high retention, corresponding to the retention property of NF membranes. Only a slight decline in dyes rejection occurred with the hybrid membranes in the filtration of negative dyes solution compared with that of

DOI: 10.1021/acssuschemeng.5b00006
ACS Sustainable Chem. Eng. 2015, 3, 690−701

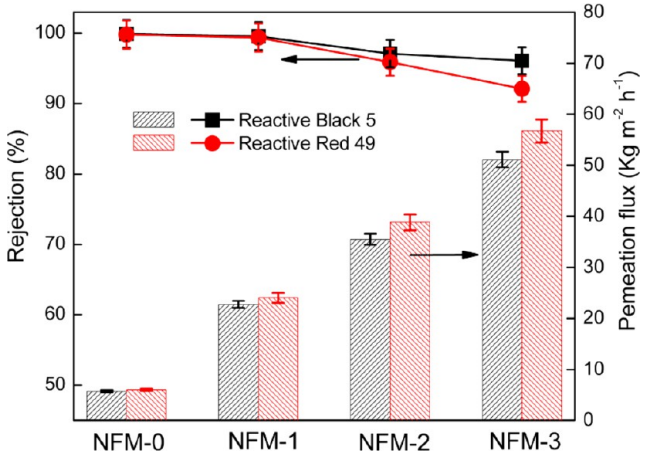

Figure 9. Flux and rejection of the loose nanofiltration membranes for Reactive Black 5 and Reactive Red 49 (0.4 MPa, 25 °C).

unfilled PES membrane, demonstrating a favorable retention performance. The explanation was as follows: the combination of a relative loose structure and positive SNPs exhibited on the top layer prompted a trace amount of negative dyes to pass through membranes. Meanwhile, dyes permeation flux of composite membranes signaly enhanced compared with that of NFM-0. Herein, an overall flux of reactive dyes could reach a high value of 51 kg m^{-2} h^{-1} for NFM-3 at 0.4 MPa, whereas NFM-0 showed the lowest value of 7.02 kg m^{-2} h^{-1}.

After dyes solution filtration at 0.4 MPa, both unfilled membrane and composite membranes were "dyed" and the effective area presented the corresponding color. To further study adsorption mechanism, the dyed membranes (NFM-0, NFM-2) were immersed in NaOH solution (0.5 mol L^{-1}) for 72 h. It was found that dyes adsorbed on the surface of NFM-0 were cleared out, while NFM-2 still remained the corresponding color. The negatively charged dyes were rejected or embedded on the membrane surface through the sieving effect under continuous pressure, and unstable dye molecules layer were formed on membrane surface. However, the hybrid membranes with positively SNPs can absorb negatively charged dyes via electrostatic interaction, giving rise to a tightly dye layer, which in turn functioned as a thin filter cake. A continuous high permeation flux obtained by experimental data demonstrated that the hybrid membranes showed a low fouling tendency. The schematic diagram is shown in Figure 10. In conclusion, the hybrid membranes exhibited both admirable rejection and high permeation flux of dyes solution. As previously mentioned, two factors, hydrophilicity and loose structure could promote permeation flux, thus notably according with the results of water contact and water ratio.

Figure 11 represents a plot of rejections to these various saline solutions (Na_2SO_4, $MgSO_4$, NaCl and $MgCl_2$, respectively) of the as-prepared membranes. For NFM-0, it was seen that the salt rejection order was Na_2SO_4 > $MgSO_4$ > $MgCl_2$ > NaCl. The rejection order showed that the unfilled membrane surface was negatively charged. In view of the negatively charged NFM-0, the rejection of Na_2SO_4 was as low as 40.7%. This may be due to the relative loose structure ascribed by direct phase inversion in comparison to the dense membrane prepared by surface modification (IP).[45,46] A similar retention of multivalent salts (Na_2SO_4) for the PES NF membrane has been reported.[39] In view of composite membranes, there are normally three types of polymer/particle

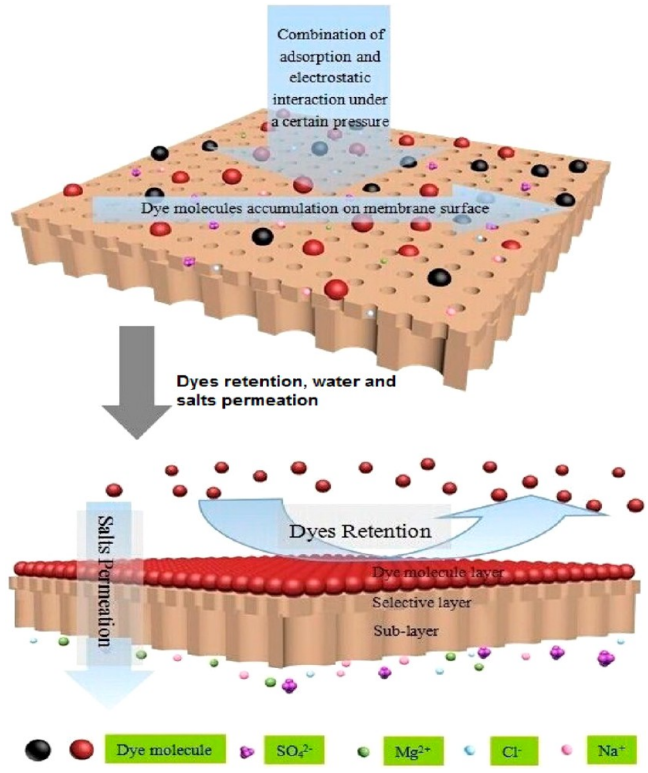

Figure 10. Schematic diagram of separation of dyes and salts for the hybrid membranes.

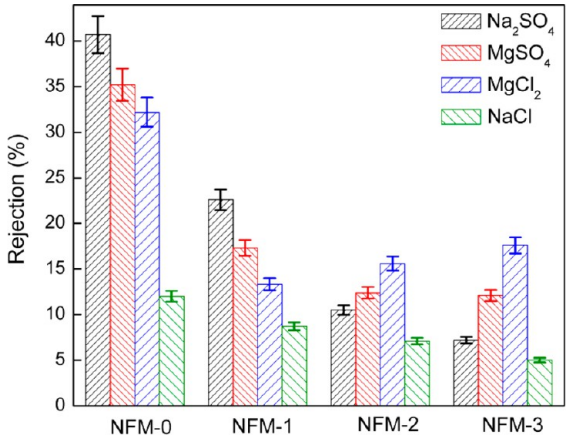

Figure 11. Effect of PEI additive amount on rejection of mono- and bivalent salts for NFM-0, NFM-1, NFM-2 and NFM-3 (0.4 MPa, 25 °C).

interfaces, that is, ideal morphology, rigidified polymer layer and interface voids,[59,60] which are shown in Figure 12. The rigidified layer is formed when the particles directly contact the polymer chains whose mobility is inhibited to a great extent, thus enhancing the overall selectivity and mechanical property of the composite membrane.[61] When the polymer/filler compatibility and adhesion are poor, the bulk polymer was disturbed and detached around hard inorganic particles, resulting in interface voids in the composite membrane.[62] In our previous work, we have prepared organic/inorganic composite membranes by blending with halloysite nanotubes (HNTs) bearing polymer brushes, which exhibited the similarly low rejections of salts. It is generally known that the improved transport properties of composite membrane are fairly

DOI: 10.1021/acssuschemeng.5b00006
ACS Sustainable Chem. Eng. 2015, 3, 690−701

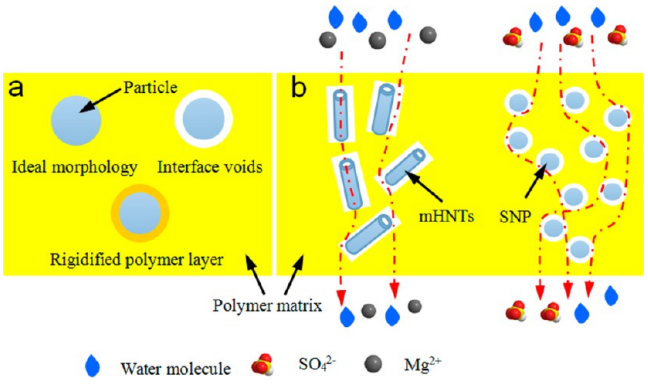

Figure 12. (a) Schematic diagram of different types of polymer/particle interfaces in composite membrane, (b) transport channels for water molecules and salts ions in two composite membranes.

influenced by the filler morphology and size, filler/polymer interface compatibility and adhesion. The poor soft polymer/modified HNTs (mHNTs) contact leads to large interface voids (Figure 12b), which in turn facilitate water or salts permeation. Herein, although a better compatibility between SNPs and polymer resulted in a stronger interface adhesion, thus decreasing interface voids volume around SNPs, hydrophilic group of SNPs could accelerate water inflow during phase inversion, causing a certain level of interface voids in the vicinity of SNPs. In this case, composite membranes containing a looser interface structure than that of unfilled membrane are capable of promoting water and hydrated ion transport. However, with an increase of PEI content, the sequence of salts retention changed: $MgCl_2$ > $MgSO_4$ > Na_2SO_4 > NaCl (NFM-2 and NFM-3). It could be explained by positively SNPs from membrane surface (Figure 4c,d), rendering membrane positively charged. Hereinto, the rejection of $MgCl_2$ and $MgSO_4$ slightly enhanced with increasing the PEI content due to an improved IEC of composite membrane, leading to more electrostatic repulsion between bivalent co-ion (Mg^{2+}) and membrane surface. It was notably, that the retention of Na_2SO_4 decreased from 22.6% (NFM-1) to 7.2% (NFM-3). Similarly, SO_4^{2-}, as a counterion, tended to pass through a positively charged channel, that is, the Donnan effect gradually occupied the dominant role in view of salts rejection. A conclusion can be drawn that the composite membranes presented excellent retention of LMW dyes and low multivalent salts retention, demonstrating an impressive prospect for dye purification and desalination.

Antifouling Performance of Membranes. The performance of membrane filtration, including target separation, permeation and long-term stability, depends greatly on the antifouling property. Composite membranes used in wastewater were easily compromised from membrane fouling ascribed to foulants adsorption and aggregation on hydrophobic membrane surface, thereby notably causing a decline in permeation flux, in view of membrane fouling caused by protein adsorption, derived from the combination of electrostatic interaction, hydrogen bonding effect, hydrophobic impact and van der Waals force.[35] Therefore, an ideal type of composite membrane should possess the following performance: high water flux, low fouling tendency and a high-efficient separation property. In this work, BSA solution (pH = 7.5) was chosen as a model protein. The sizes of the BSA molecules were larger than the pore sizes of all membranes. Hence, foulants could not penetrate into the pores and merely generated biofouling for the membrane surface. The antifouling performance of unfilled PES and composite membrane was analyzed by measuring the water flux recovery after the membrane was contaminated by BSA solution.

Figure 13a presents the permeation flux of tested membranes before and after protein filtration. Herein, water flux of the fouled membranes were measured followed by filtration with DI water for 30 min. As seen from Figure 13, the flux decreased distinctly when pure water was replaced by protein solution, which was caused by the combination of concentration polarization and membrane fouling. After washing the membranes, the flux recovered to a stable high-level for the hybrid membranes. However, the unfilled PES membranes exhibited a large decline of the pure water flux. And flux recovery ratio was calculated to evaluate the antifouling performance of the membranes.

The total flux decline ratio (R_t) and flux recovery ratio (FRR) of the tested membranes are presented in Figure 13b. It was widely accepted that the higher FRR indicated a better antifouling property for the membrane. The FRR was as low as 56.5% for unfilled PES membrane, whereas the composite membranes containing hydrophilic SNPs showed an overall high value of over 75%. Especially for NFM-3, the flux recovery percentage reached as high as 94.5%. These results showed an

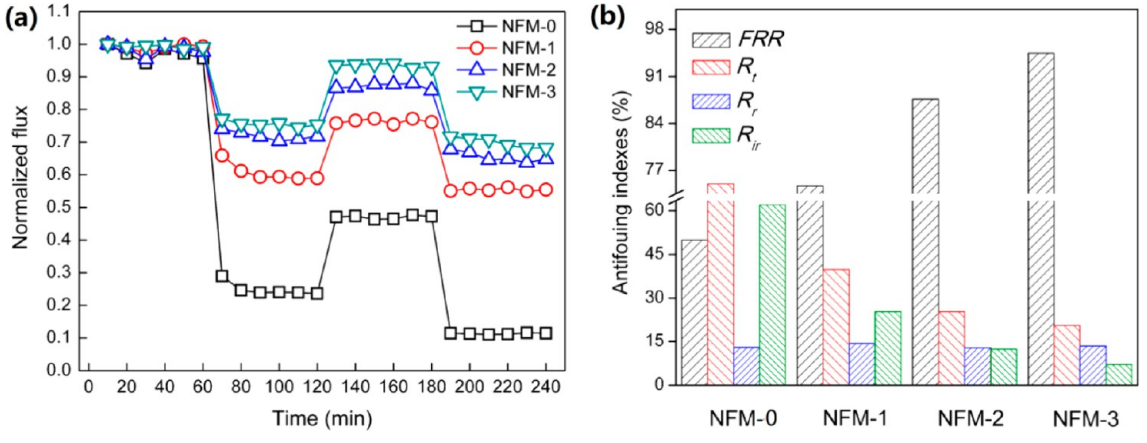

Figure 13. (a) Normalized flux of the pristine and hybrid membranes during the filtration of BSA solution (0.4 MPa, 25 °C), (b) fouling resistance ratio of PEI nanoparticles blended PES membranes affected by different PEI concentration.

DOI: 10.1021/acssuschemeng.5b00006
ACS Sustainable Chem. Eng. 2015, 3, 690−701

excellent antifouling performance of the composite membranes. As earlier mentioned, composite membrane surface could absorb water molecules and form a tightly water layer, which retarded foulant adsorption.[63] Although BSA was negatively charged, giving rise to electrostatic interaction between BSA and membrane surface in the filtration of BSA solution, the large size restrict its penetration into membrane matrix. When washed with DI water, the foulant deposition could be taken away by DI water due to the rigorous disturbance near the hydrophilic membrane surface. The R_t of the neat membrane was quite high (75%) during the filtration of BSA solution, indicating a inferior antifouling property. From Figure 13b, the irreversible fouling ratio (R_{ir}) of the membranes considerably reduced from 62% of NFM-0 to 7.1% of NFM-3. Irreversible fouling, in which the foulants were tightly attached to the membrane and they were hardly to be removed by facile washing. The results showed that NFM-3 had an excellent antifouling ability, which promoted a further practical application in dye purification and desalination. In summary, the antifouling properties of hybrid membranes were greatly improved, i.e., the surface performance of the hybrid membranes was successfully optimized.

CONCLUSIONS

A novel method for fabricating composite membranes was the in situ synthesis of SNPs in the process of forming PES casting solution. The composite membranes containing hydrophilic SNPs exhibited a substantially enhanced surface hydrophilicity and charge density, facilitating the antifouling property of hybrid membranes. The water flux of composite membranes has achieved as high as 75.37 L m^{-2} h^{-1} at 0.6 MPa. This was due to the combination of relative loose interface structure and high membrane hydrophilicity. It was observed that increasing the PEI content from 0 to 1.5 wt % reduced the R_{ir} from 62% to 7.07% for NFM-3, demonstrating a fairly high antifouling performance. In brief, the as-prepared membranes with high retention of LMW dyes and salts permeation, and antifouling tendency will broaden their wide applicant in the treatment of dye purification and desalination.

AUTHOR INFORMATION

Corresponding Authors

*Y. Zhang. Tel.: +86-371-67781734. Fax: +86-371-67739348. E-mail: zhangyatao@zzu.edu.cn.

*J. Liu. E-mail: liujindun@zzu.edu.cn.

Notes

The authors declare no competing financial interest.

ACKNOWLEDGMENTS

We gratefully acknowledge the support from the National Natural Science Foundation of China (Nos. 21476215 and 21376225), and Excellent Youth Development Foundation of Zhengzhou University (No. 1421324066). We sincerely acknowledge the financial assistance of visiting research program in the University of New South Wales by the China Scholarship Council (No. 201208410135).

REFERENCES

(1) Rafatullah, M.; Sulaiman, O.; Hashim, R.; Ahmad, A. Adsorption of methylene blue on low-cost adsorbents: a review. *J. Hazard. Mater.* **2010**, *177* (1−3), 70−80.

(2) Wu, J.; Wang, J.; Li, H.; Du, Y.; Huang, K.; Liu, B. Designed synthesis of hematite-based nanosorbents for dye removal. *J. Mater. Chem. A* **2013**, *1* (34), 9837−9847.

(3) Körbahti, B. K.; Artut, K.; Geçgel, C.; Özer, A. Electrochemical decolorization of textile dyes and removal of metal ions from textile dye and metal ion binary mixtures. *Chem. Eng. J.* **2011**, *173* (3), 677−688.

(4) Forgacs, E.; Cserhati, T.; Oros, G. Removal of synthetic dyes from wastewaters: a review. *Environ. Int.* **2004**, *30* (7), 953−971.

(5) Verma, A. K.; Dash, R. R.; Bhunia, P. A review on chemical coagulation/flocculation technologies for removal of colour from textile wastewaters. *J. Environ. Manage.* **2012**, *93* (1), 154−168.

(6) Geng, Z.; Lin, Y.; Yu, X.; Shen, Q.; Ma, L.; Li, Z.; Pan, N.; Wang, X. Highly efficient dye adsorption and removal: A functional hybrid of reduced graphene oxide−Fe_3O_4 nanoparticles as an easily regenerative adsorbent. *J. Mater. Chem.* **2012**, *22* (8), 3527−3535.

(7) Robinson, T.; McMullan, G.; Marchant, R.; Poonam, N. Remediation of dyes in textile effluent: A critical review on current treatment technologies with a proposed alternative. *Bioresour. Technol.* **2001**, *77*, 247−255.

(8) Wang, X. S.; Zhou, Y.; Jiang, Y.; Sun, C. The removal of basic dyes from aqueous solutions using agricultural by-products. *J. Hazard. Mater.* **2008**, *157* (2−3), 374−385.

(9) Zhao, L.; Chen, X.; Wang, X.; Zhang, Y.; Wei, W.; Sun, Y.; Antonietti, M.; Titirici, M. M. One-step solvothermal synthesis of a carbon@TiO_2 dyade structure effectively promoting visible-light photocatalysis. *Adv. Mater.* **2010**, *22* (30), 3317−3321.

(10) Laohhasurayotin, K.; Viboonratanasri, D. Preparation and characterization of titania-entrapped silica hollow particles: Effective dye removal and evidence of selectivity. *Phys. Chem. Chem. Phys.* **2013**, *15* (24), 9626−9635.

(11) Liu, Y.; Zhang, S.; Zhou, Z.; Ren, J.; Geng, Z.; Luan, J.; Wang, G. Novel sulfonated thin-film composite nanofiltration membranes with improved water flux for treatment of dye solutions. *J. Membr. Sci.* **2012**, *394*−*395*, 218−229.

(12) Dou, X.; Li, P.; Zhang, D.; Feng, C.-L. C_2-symmetric benzene-based hydrogels with unique layered structures for controllable organic dye adsorption. *Soft Matter* **2012**, *8* (11), 3231−3238.

(13) Li, X.; Chen, Y.; Hu, X.; Zhang, Y.; Hu, L. Desalination of dye solution utilizing PVA/PVDF hollow fiber composite membrane modified with TiO_2 nanoparticles. *J. Membr. Sci.* **2014**, *471*, 118−129.

(14) Yu, S.; Gao, C.; Su, H.; Liu, M. Nanofiltration used for desalination and concentration in dye production. *Desalination* **2001**, *140*, 97−100.

(15) He, Y.; Li, G.; Wang, H.; Zhao, J.; Su, H.; Huang, Q. Effect of operating conditions on separation performance of reactive dye solution with membrane process. *J. Membr. Sci.* **2008**, *321* (2), 183−189.

(16) Wang, L.; Ji, S.; Wang, N.; Zhang, R.; Zhang, G.; Li, J.-R. One-step self-assembly fabrication of amphiphilic hyperbranched polymer composite membrane from aqueous emulsion for dye desalination. *J. Membr. Sci.* **2014**, *452*, 143−151.

(17) Han, R.; Zhang, S.; Xing, D.; Jian, X. Desalination of dye utilizing copoly(phthalazinone biphenyl ether sulfone) ultrafiltration membrane with low molecular weight cut-off. *J. Membr. Sci.* **2010**, *358* (1−2), 1−6.

(18) Vandezande, P.; Gevers, L. E.; Vankelecom, I. F. Solvent resistant nanofiltration: Separating on a molecular level. *Chem. Soc. Rev.* **2008**, *37* (2), 365−405.

(19) Sotto, A.; Boromand, A.; Balta, S.; Kim, J.; Van der Bruggen, B. Doping of polyethersulfone nanofiltration membranes: Antifouling effect observed at ultralow concentrations of TiO_2 nanoparticles. *J. Mater. Chem.* **2011**, *21* (28), 10311−10320.

(20) Xie, W.; He, F.; Wang, B.; Chung, T.-S.; Jeyaseelan, K.; Armugam, A.; Tong, Y. W. An aquaporin-based vesicle-embedded polymeric membrane for low energy water filtration. *J. Mater. Chem. A* **2013**, *1* (26), 7592−7600.

DOI: 10.1021/acssuschemeng.5b00006
ACS Sustainable Chem. Eng. 2015, 3, 690−701

(21) Liu, Z.; Bai, H.; Lee, J.; Sun, D. D. A low-energy forward osmosis process to produce drinking water. *Energy Environ. Sci.* **2011**, *4* (7), 2582−2585.
(22) Lin, J. Y.; Ye, W. Y.; Zeng, H. M.; Yong, H.; Shen, J. N.; Darvishmanesh, S.; Luis, L.; Sotto, A.; Van der Bruggen, B. Fractionation of direct dyes and salts in aqueous solution using loose nanofiltration Membranes. *J. Membr. Sci.* **2015**, *477*, 183−193.
(23) Zhong, P. S.; Widjojo, N.; Chung, T.-S.; Weber, M.; Maletzko, C. Positively Charged Nanofiltration (NF) membranes *via* UV grafting on sulfonated polyphenylenesulfone (sPPSU) for effective removal of textile dyes from wastewater. *J. Membr. Sci.* **2012**, *417−418*, 52−60.
(24) Sun, S. P.; Hatton, T. A.; Chung, T. S. Hyperbranched polyethyleneimine induced cross-linking of polyamide-imide nanofiltration hollow fiber membranes for effective removal of ciprofloxacin. *Environ. Sci. Technol.* **2011**, *45* (9), 4003−4009.
(25) Shao, L.; Cheng, X. Q.; Liu, Y.; Quan, S.; Ma, J.; Zhao, S. Z.; Wang, K. Y. Newly developed nanofiltration (NF) composite membranes by interfacial polymerization for safranin O and aniline blue removal. *J. Membr. Sci.* **2013**, *430*, 96−105.
(26) Chidambaram, T.; Oren, Y.; Noel, M. Fouling of nanofiltration membranes by dyes during brine recovery from textile dye bath. *Chem. Eng. J.* **2015**, *262*, 156−168.
(27) Ong, Y. K.; Li, F. Y.; Sun, S.-P.; Zhao, B. W.; Liang, C.-Z.; Chung, T.-S. Nanofiltration hollow fiber membranes for textile wastewater treatment: Lab-scale and pilot-scale studies. *Chem. Eng. Sci.* **2014**, *114*, 51−57.
(28) Ji, Y.-L.; An, Q.-F.; Zhao, Q.; Sun, W.-D.; Lee, K.-R.; Chen, H.-L.; Gao, C.-J. Novel composite nanofiltration membranes containing zwitterions with high permeate flux and improved anti-fouling performance. *J. Membr. Sci.* **2012**, *390−391*, 243−253.
(29) Fan, X.; Dong, Y.; Su, Y.; Zhao, X.; Li, Y.; Liu, J.; Jiang, Z. Improved performance of composite nanofiltration membranes by adding calcium chloride in aqueous phase during interfacial polymerization Process. *J. Membr. Sci.* **2014**, *452*, 90−96.
(30) Song, J. F.; Li, X.-M.; Li, Z. S.; Zhang, M. X.; Yin, Y.; Zhao, B. L.; Chen, G.; Kong, D. F.; He, T. Stabilization of composite hollow fiber nanofiltration membranes with a sulfonated poly(ether ether ketone) coating. *Desalination* **2015**, *355*, 83−90.
(31) Zhu, J. Y.; Tian, M. M.; Zhang, Y. T.; Zhang, H. Q.; Liu, J. D. Fabrication of a novel "loose" nanofiltration membrane by facile blending with chitosan-montmorillonite nanosheets for dyes purification. *Chem. Eng. J.* **2015**, *265*, 184−193.
(32) Sun, S. P.; Hatton, T. A.; Chan, S. Y.; Chung, T.-S. Novel thin-film composite nanofiltration hollow fiber membranes with double repulsion for effective removal of emerging organic matters from water. *J. Membr. Sci.* **2012**, *401−402*, 152−162.
(33) Zheng, Y.; Yao, G.; Cheng, Q.; Yu, S.; Liu, M.; Gao, C. Positively charged thin-film composite hollow fiber nanofiltration membrane for the removal of cationic dyes through submerged filtration. *Desalination* **2013**, *328*, 42−50.
(34) Zhu, J. Y.; Guo, N. N.; Zhang, Y. T.; Yu, L.; Liu, J. D. Preparation and characterization of negatively charged PES nanofiltration membrane by blending with halloysite nanotubes grafted with poly(sodium 4-styrenesulfonate) *via* surface-initiated ATRP. *J. Membr. Sci.* **2014**, *465*, 91−99.
(35) Zhao, C.; Xue, J.; Ran, F.; Sun, S. Modification of polyethersulfone membranes—A review of methods. *Prog. Mater. Sci.* **2013**, *58* (1), 76−150.
(36) Li, S.; Liao, G.; Liu, Z.; Pan, Y.; Wu, Q.; Weng, Y.; Zhang, X.; Yang, Z.; Tsui, O. K. C. Enhanced water flux in vertically aligned carbon nanotube arrays and polyethersulfone composite membranes. *J. Mater. Chem. A* **2014**, *2* (31), 12171−12176.
(37) Zhu, L.-J.; Zhu, L.-P.; Zhao, Y.-F.; Zhu, B.-K.; Xu, Y.-Y. Antifouling and anti-bacterial polyethersulfone membranes quaternized from the additive of poly(2-dimethylamino ethyl methacrylate) grafted SiO_2 nanoparticles. *J. Mater. Chem. A* **2014**, *2* (37), 15566−15574.
(38) Bernstein, R.; Anton, E.; Ulbricht, M. UV-photo graft functionalization of polyethersulfone membrane with strong polyelectrolyte hydrogel and its application for nanofiltration. *ACS Appl. Mater. Interfaces* **2012**, *4* (7), 3438−3446.
(39) Vatanpour, V.; Madaeni, S. S.; Moradian, R.; Zinadini, S.; Astinchap, B. Fabrication and characterization of novel antifouling nanofiltration membrane prepared from oxidized multiwalled carbon nanotube/polyethersulfone nanocomposite. *J. Membr. Sci.* **2011**, *375* (1−2), 284−294.
(40) Vatanpour, V.; Madaeni, S. S.; Moradian, R.; Zinadini, S.; Astinchap, B. Novel antibifouling nanofiltration polyethersulfone membrane fabricated from embedding TiO_2 coated multiwalled carbon nanotubes. *Sep. Purif. Technol.* **2012**, *90*, 69−82.
(41) Ba, C.; Ladner, D. A.; Economy, J. Using polyelectrolyte coatings to improve fouling resistance of a positively charged nanofiltration membrane. *J. Membr. Sci.* **2010**, *347* (1−2), 250−259.
(42) He, T.; Frank, M.; Mulder, M. H. V.; Wessling, M. Preparation and characterization of nanofiltration membranes by coating polyethersulfone hollow fibers with sulfonated poly(ether ether ketone) (SPEEK). *J. Membr. Sci.* **2008**, *307* (1), 62−72.
(43) Deng, H.; Xu, Y.; Chen, Q.; Wei, X.; Zhu, B. High flux positively charged nanofiltration membranes prepared by UV-initiated graft polymerization of methacrylatoethyl trimethyl ammonium chloride (DMC) onto polysulfone membranes. *J. Membr. Sci.* **2011**, *366* (1−2), 363−372.
(44) Wang, X.; Wei, J.; Dai, Z.; Zhao, K.; Zhang, H. Preparation and characterization of negatively charged hollow fiber nanofiltration membrane by plasma-induced graft polymerization. *Desalination* **2012**, *286*, 138−144.
(45) An, Q.-F.; Sun, W.-D.; Zhao, Q.; Ji, Y.-L.; Gao, C.-J. Study on a novel nanofiltration membrane prepared by interfacial polymerization with zwitterionic amine monomers. *J. Membr. Sci.* **2013**, *431*, 171−179.
(46) Fang, W.; Shi, L.; Wang, R. Interfacially polymerized composite nanofiltration hollow fiber membranes for low-pressure water softening. *J. Membr. Sci.* **2013**, *430*, 129−139.
(47) Fu, Q.; Wong, E. H. H.; Kim, J.; Scofield, J. M. P.; Gurr, P. A.; Kentish, S. E.; Qiao, G. G. The effect of soft nanoparticles morphologies on thin film composite membrane performance. *J. Mater. Chem. A* **2014**, *2* (42), 17751−17756.
(48) Li, Y.; He, G.; Wang, S.; Yu, S.; Pan, F.; Wu, H.; Jiang, Z. Recent advances in the fabrication of advanced composite membranes. *J. Mater. Chem. A* **2013**, *1* (35), 10058−10077.
(49) Halim, A.; Fu, Q.; Yong, Q.; Gurr, P. A.; Kentish, S. E.; Qiao, G. G. Soft polymeric nanoparticle additives for next generation gas separation membranes. *J. Mater. Chem. A* **2014**, *2* (14), 4999−5009.
(50) Kotte, M. R.; Cho, M.; Diallo, M. S. A facile route to the preparation of mixed matrix polyvinylidene fluoride membranes with in-situ generated polyethyleneimine particles. *J. Membr. Sci.* **2014**, *450*, 93−102.
(51) Chen, Y.; Zhang, Y.; Liu, J.; Zhang, H.; Wang, K. Preparation and antibacterial property of polyethersulfone ultrafiltration hybrid membrane containing halloysite nanotubes loaded with copper ions. *Chem. Eng. J.* **2012**, *210*, 298−308.
(52) Yu, H.; Zhang, X.; Zhang, Y.; Liu, J.; Zhang, H. Development of a hydrophilic PES ultrafiltration membrane containing SiO_2@N-halamine nanoparticles with both organic antifouling and antibacterial properties. *Desalination* **2013**, *326*, 69−76.
(53) Yu, L.; Zhang, Y.; Zhang, B.; Liu, J.; Zhang, H.; Song, C. Preparation and characterization of HPEI-GO/PES ultrafiltration membrane with antifouling and antibacterial properties. *J. Membr. Sci.* **2013**, *447*, 452−462.
(54) Xu, Z.; Zhang, J.; Shan, M.; Li, Y.; Li, B.; Niu, J.; Zhou, B.; Qian, X. Organosilane-functionalized graphene oxide for enhanced antifouling and mechanical properties of polyvinylidene fluoride ultrafiltration membranes. *J. Membr. Sci.* **2014**, *458*, 1−13.
(55) Han, M.-J.; Nam, S.-T. Thermodynamic and rheological variation in polysulfone solution by PVP and its effect in the preparation of phase inversion membrane. *J. Membr. Sci.* **2002**, *202*, 55−61.
(56) Liu, M.; Zhou, C.; Dong, B.; Wu, Z.; Wang, L.; Yu, S.; Gao, C. Enhancing the permselectivity of thin-film composite poly(vinyl

DOI: 10.1021/acssuschemeng.5b00006
ACS Sustainable Chem. Eng. 2015, 3, 690−701

alcohol) (PVA) nanofiltration membrane by incorporating poly-(sodium-p-styrene-sulfonate) (PSSNa). *J. Membr. Sci.* **2014**, *463*, 173−182.
(57) Chen, Y.; Zhang, Y.; Zhang, H.; Liu, J.; Song, C. Biofouling control of halloysite nanotubes-decorated polyethersulfone ultrafiltration membrane modified with chitosan-silver nanoparticles. *Chem. Eng. J.* **2013**, *228*, 12−20.
(58) Yu, H.; Zhang, Y.; Sun, X.; Liu, J.; Zhang, H. Improving the antifouling property of polyethersulfone ultrafiltration membrane by incorporation of dextran grafted halloysite nanotubes. *Chem. Eng. J.* **2014**, *237*, 322−328.
(59) Moore, T. T.; Koros, W. J. Non-ideal effects in organic−inorganic materials for gas separation membranes. *J. Mol. Struct.* **2005**, *739* (1−3), 87−98.
(60) Vu, D. Q.; Koros, W. J.; Miller, S. J. Mixed matrix membranes using carbon molecular sieves I. Preparation and experimental results. *J. Membr. Sci.* **2003**, *211*, 311−334.
(61) Moore, T. T.; Mahajan, R.; Vu, D. Q.; Koros, W. J. Hybrid membrane materials comprising organic polymers with rigid dispersed phases. *AIChE J.* **2004**, *50*, 311−321.
(62) Chung, T.-S.; Jiang, L. Y.; Li, Y.; Kulprathipanja, S. Mixed matrix membranes (MMMs) comprising organic polymers with dispersed inorganic fillers for gas separation. *Prog. Polym. Sci.* **2007**, *32* (4), 483−507.
(63) Zinadini, S.; Zinatizadeh, A. A.; Rahimi, M.; Vatanpour, V.; Zangeneh, H. Preparation of a novel antifouling mixed matrix PES membrane by embedding graphene oxide nanoplates. *J. Membr. Sci.* **2014**, *453*, 292−301.

DOI: 10.1021/acssuschemeng.5b00006
ACS Sustainable Chem. Eng. 2015, 3, 690−701